
ρ -GNF : A Novel Sensitivity Analysis Approach Under Unobserved Confounders

Sourabh Balgi*

Department of Computer and Information Science (IDA)
Linköping University
Linköping, Sweden
sourabh.balgi@liu.se

Jose M. Peña

Department of Computer and Information Science (IDA)
Linköping University
Linköping, Sweden
jose.m.pena@liu.se

Adel Daoud

Institute for Analytical Sociology (IAS)
Linköping University
Linköping, Sweden
adel.daoud@liu.se

Abstract

We propose a new sensitivity analysis model that combines copulas and normalizing flows for causal inference under unobserved confounding. We refer to the new model as ρ -GNF (ρ -Graphical Normalizing Flow), where $\rho \in [-1, +1]$ is a bounded sensitivity parameter representing the backdoor non-causal association due to unobserved confounding modeled using the most well studied and widely popular Gaussian copula. Specifically, ρ -GNF enables us to estimate and analyse the frontdoor causal effect or average causal effect (ACE) as a function of ρ . We call this the ρ_{curve} . The ρ_{curve} enables us to specify the confounding strength required to nullify the ACE. We call this the ρ_{value} . Further, the ρ_{curve} also enables us to provide bounds for the ACE given an interval of ρ values. We illustrate the benefits of ρ -GNF with experiments on simulated and real-world data in terms of our empirical ACE bounds being narrower than other popular ACE bounds.

1 Introduction

The main objectives of causal inference are the identification and estimation of the effect of a treatment on an outcome. As these objectives are an integral part of any applied discipline (e.g., economics, epidemiology, sociology) that aims to analyze cause and effect in a domain of interest (e.g., poverty, medicine, inequality), much attention is spent on improving existing and developing new causal inference methods—especially, tailoring them for the age of big data and personalized treatments.

In terms of the identification and estimation of the causal effect, randomized controlled trials (RCTs) are celebrated as the *Gold Standard* of research designs as they require the least assumptions [20]. An RCT guarantees unconfoundedness (also known as ignorability or exchangability) critical for the

*Contact author

causal effect identification due to random treatment assignment [63, 66, 68]. *Unconfoundedness* means that there are no unobserved common causes (i.e., confounders) between the treatment and the outcome. Thus, when unconfoundedness holds, an association (correlation) does imply causation. Despite that a successful RCT enables the identification and estimation of the causal effect, RCTs may be infeasible, unethical, or expensive to execute properly. Hence, there is a need to continue developing causal inference methods for observational (non-randomized) data.

If an RCT provides unconfoundedness by construction, observational studies requires that unconfoundedness holds by assumption [3, 66, 68]. Identifying a causal effect is not possible to achieve under unobserved confounding, because one needs to adjust for all the non-causal backdoor paths, and that requires all the confounders being observed [26, 55, 72, 82]. When there remains unobserved confounding between the treatment and outcome, techniques such as instrumental variables [1, 28] or the front-door criterion [56, 65] have proven useful as they assume alternate forms of unconfoundedness. Despite their usefulness, they merely shift the unconfoundedness assumption alternate forms from referring between *the treatment and the outcome* (in the case of directly adjusting for confounders) to either between *the treatment's parent and the outcome* (i.e., *instrumental variable*) or between *the treatment's child and the outcome* (i.e., *front-door criterion*). Hence, causal effect identification in observational studies necessitates the unconfoundedness assumption to hold at least in some part of the causal system of interest.

Because the unconfoundedness assumption is so critical and at the same time untestable in observational studies [68], there exist several frameworks for stress testing causal effect estimates. These tests offer frameworks that account for what occurs with the point estimate under different degrees of unconfoundedness failure. These sort of tests have been termed as '*sensitivity analysis*' in the causal inference literature [6, 27, 42, 71, 84] (also known as '*bias analysis*' [9, 10, 36, 67] in epidemiology). The *degree of unconfoundedness failure* corresponds to the strength to which an unobserved confounding affects the treatment and outcome.

The current sensitivity analysis literature can be roughly categorized into two streams: (i) identify the '*bounds*' of the causal effect as functions of some sensitivity parameters [15, 27, 42, 58, 64, 73, 75, 84]; and (ii) identify how large the influence of the unobserved confounders needs to be to '*explain-away*' the causal effect [74, 85, 86]. While some bounds methods provide assumption-free (hereon referred as AF) bounds of the causal effect for binary treatment and outcome [15, 42, 64], other methods provide bounds as functions of sensitivity parameters to be tuned by a domain expert [58, 73, 75]. The term *assumption free* means that the domain expert does not have to do any distributional assumption about how the confounder affects the treatment and outcome. In contrast to the '*bounds*' stream, there are methods that fall under the other '*explain-away*' stream where the E-value [85] (hereon referred as VW [85] for VanderWeele) is proposed as the minimum strength of the unmeasured confounder that is needed, conditional on the measured confounders, to fully explain-away a specific treatment-outcome causal association [74, 85, 86]. Similar to the E-value, the recently developed '*Austen plots*' [86] identify the influence of the confounding needed to explain-away a specific amount of bias in the causal effect estimate. Other studies combine both bounds and explain-away methods [73].

At least two problems remain open in the sensitivity analysis literature. First, existing methods require that the domain expert specify several abstract sensitivity parameters, which may be difficult to reason about in concrete settings. Second, while existing methods have addressed the unconfoundedness in a relatively simple setting of binary outcomes, the problem of unconfoundedness in observational studies still largely remains to be addressed for the general cases of non-binary outcomes. More specifically, even though the AF bounds ensure the existence of the true ACE in their bound range [42, 64], they are often too wide and uninformative for assessing if the ACE is positive, zero, or negative. VW [85] propose identifying bounds under the assumption that the domain expert provides values for three sensitivity parameters that represent the confounding strength to produce narrower intervals than AF. However, as shown by Sjölander [73], the VW can under certain conditions defeat its purpose and produce wider bounds than AF. This wideness can occur even when the sensitivity parameters are correctly chosen. Thus, VW bounds are not always sharp, i.e., they are unattainable under some circumstances. Additionally, these AF and VW bounds apply only for binary outcomes, thus limiting their applicability. Consequently, if there was a method that would address these two limitations, domains experts would be in a better position to cover new scientific ground.

To address the two open problems mentioned above, we develop a new sensitivity analysis method that allows the domain expert to supply more concrete knowledge in the form of copula than VW's

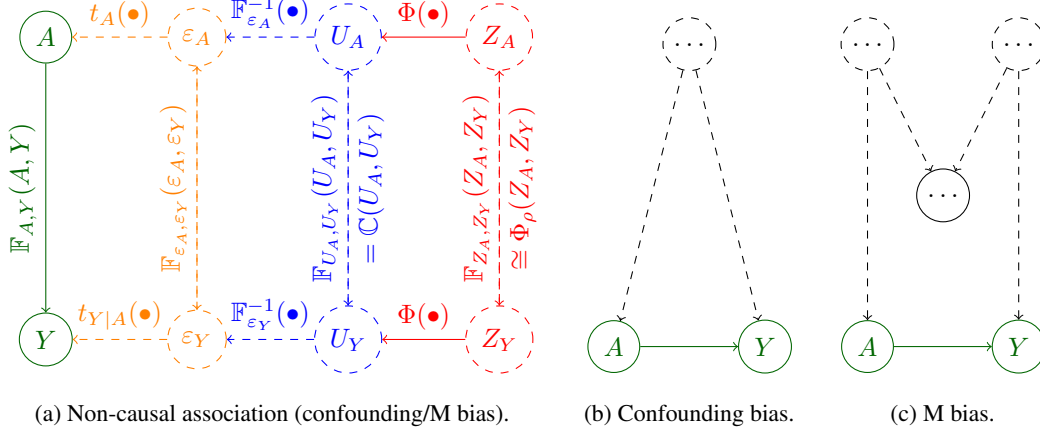


Figure 1: (a) Observationally and interventionally equivalent SCM representations of the observed treatment (cause) A and outcome (effect) Y in terms of transformations $\{t_{X|X_{pa}}(\bullet), \mathbb{F}_{X|X_{pa}}^{-1}(\bullet) = t_{X|X_{pa}}(\mathbb{F}_{\varepsilon_X}^{-1}(\bullet)), \mathbb{T}_{X|X_{pa}}(\bullet) = t_{X|X_{pa}}(\mathbb{F}_{\varepsilon_X}^{-1}(\Phi(\bullet)))\}$ of their respective unobserved SCM noises $\{\varepsilon_X, U_X, Z_X\}$, where variable $X \in \{A, Y\}$ and X_{pa} is the set of observed parent of X . The solid-lined nodes/edges indicate treatment/outcome variables and the dash-lined nodes/edges indicate unobserved noise variables. The green, orange, blue and red lines respectively indicate the frontdoor causal association $A \rightarrow Y$, non-causal association due to noises ε_X , non-causal association due to uniform marginal noises $U_X \in [0, 1]$, non-causal association due to Gaussian marginal noises Z_X . (b, c) From the observational and interventional equivalence results of SCMs [45, 47, 59], it follows that the backdoor non-causal association due to confounding and/or M bias can be represented as the SCM representation in (a).

abstract parameters for creating narrower ACE bounds. Our method enables the domain expert to encode the confounding strength by reasoning about the joint distribution of the treatment, outcome, and confounding. That reasoning translates to choosing an appropriate copula rather than to specifying sensitivity analysis parameters. The first benefit is that unlike VW [85], our method always produces sharp bounds, and thus, narrower intervals than AF bounds. The second benefit is that unlike AF and VW [85] bounds, our method works for discrete and continuous outcomes. In summary, our method complements VW [85] by giving the user an alternative way of encoding the strength of confounding in terms of different distributions using copulas.

Our method development consists of the following three key steps. First, we propose a new method for sensitivity analysis based on the Graphical Normalizing Flow (GNF) [88], because of GNF's attractive properties of invertibility and the similarities to most well studied and popular elliptical copula, i.e., Gaussian copula. We call our method, ρ -GNF. Here, ρ is the sensitivity parameter of the Gaussian copula representing the unobserved backdoor non-causal association between the treatment and outcome. Unlike most sensitivity analysis methods where the sensitivity parameters are unbounded and difficult to specify and interpret, ρ is bounded in the range $[-1, +1]$ as it represents the measure of dependence corresponding to the backdoor non-causal association between the treatment and outcome. Second, we show that ρ -GNF enables us to estimate a range of causal effect as a function of ρ . We call this range the ρ_{curve} , and this curve enables us to better analyze the confounding strength—under all possible degrees of unconfoundedness failure—required to explain-away the causal effect. Thus, the ρ_{curve} enables us to provide all bounds for the causal effect given an interval of ρ values that the domain expert considers appropriate. Third, we empirically demonstrate sharp and narrower bounds compared to the widely popular AF and VW bounds through simulated as well as real-world experiments that shows ρ -GNF is robust and accommodates both discrete and continuous variables.

2 Problem, Notation and Construction of ρ -GNF for Sensitivity Analysis

Let A be the treatment (or action or cause) and Y be the outcome (or effect) that constitute the observed variables with observational joint cumulative distribution function (CDF) $\mathbb{F}_{A,Y}(A, Y)$ in

Fig. 1a. Let the true Structural Causal Model (SCM) [19, 21, 22, 32, 60, 90] for the observed variables A and Y in Fig. 1a (orange) be defined as a transformation of the unobserved noises ε_A and ε_Y as

$$SCM \quad :: \quad A := t_A(\varepsilon_A) \quad , \quad Y := t_Y(A, \varepsilon_Y) = t_{Y|A}(\varepsilon_Y) \quad , \quad (1a)$$

where $(\varepsilon_A, \varepsilon_Y)$ follows the joint CDF $\mathbb{F}_{\varepsilon_A, \varepsilon_Y}(\varepsilon_A, \varepsilon_Y)$. The unobserved SCM noises $(\varepsilon_A, \varepsilon_Y)$ need not be limited only to standard normal or uniform variables and hence can be arbitrary random variables. Using the transformation of variables, the arbitrary unobserved variables ε_A and ε_Y of the *SCM* in Eq. (1a) can equivalently be written in terms of uniform unobserved variables U_A and U_Y in the interval $[0, 1]$ resulting in the *SCM* in Fig. 1a (orange+blue) as

$$SCM \quad :: \quad A := t_A(\mathbb{F}_{\varepsilon_A}^{-1}(U_A)) \quad , \quad Y := t_{Y|A}(\mathbb{F}_{\varepsilon_Y}^{-1}(U_Y)) \quad , \quad (1b)$$

where $\mathbb{F}_{\varepsilon_A}$ and $\mathbb{F}_{\varepsilon_Y}$ respectively denote the marginal distributions of ε_A and ε_Y , and (U_A, U_Y) follows the joint CDF $\mathbb{F}_{U_A, U_Y}(U_A, U_Y)$. The *SCM* in Eq. (1b) is simplified as follows in terms of \mathbb{F}_A and $\mathbb{F}_{Y|A}$ respectively defined as the marginal distributions of A and of Y conditioned on A .

$$SCM \quad :: \quad A := \mathbb{F}_A^{-1}(U_A) \quad , \quad Y := \mathbb{F}_{Y|A}^{-1}(U_Y) \quad , \quad (1c)$$

where (U_A, U_Y) follows the joint CDF $\mathbb{F}_{U_A, U_Y}(U_A, U_Y)$ with uniform marginals in $[0, 1]$. Further, we may represent the uniform unobserved variables U_A and U_Y in Eq. (1c) as transformation of standard normal unobserved variables using the CDF of the standard normal Φ in Fig. 1a (orange+blue+red) as

$$SCM \quad :: \quad A := \mathbb{F}_A^{-1}(\Phi(Z_A)) \quad , \quad Y := \mathbb{F}_{Y|A}^{-1}(\Phi(Z_Y)) \quad , \quad (1d)$$

where (Z_A, Z_Y) follows the joint CDF $\mathbb{F}_{Z_A, Z_Y}(Z_A, Z_Y)$ with standard normal marginals. Note that Eqs. (1a)-(1d) represent the same *SCM* defined in Fig. 1a, but with different unobserved noises due to the monotonic transformations $\mathbb{F}_{\varepsilon_A}^{-1}(\bullet)$, $\mathbb{F}_{\varepsilon_Y}^{-1}(\bullet)$ and $\Phi(\bullet)$. Due to the completeness of *do*-calculus [26, 72, 82], the causal effect of interest is not identifiable from any of the equivalent *SCMs* in Eqs. (1a)-(1d) unless the backdoor non-causal noise distributions are known/observed.

The result of Sklar's Theorem [76] implies that the unobserved joint CDFs $\mathbb{F}_{\varepsilon_A, \varepsilon_Y}(\varepsilon_A, \varepsilon_Y)$, $\mathbb{F}_{U_A, U_Y}(U_A, U_Y)$ and $\mathbb{F}_{Z_A, Z_Y}(Z_A, Z_Y)$ may be represented using a copula \mathbb{C} . A copula \mathbb{C} is a multivariate distribution function defined on the unit hypercube with uniform marginals [48]. As the name suggests, a copula 'ties' or 'links' or 'couples' a multidimensional distribution to its marginals. Specifically, from the scale-invariance property of copula \mathbb{C} to strictly increasing transformations $\mathbb{F}_{\varepsilon_A}$, $\mathbb{F}_{\varepsilon_Y}$, and Φ , $\mathbb{F}_{\varepsilon_A, \varepsilon_Y}(\varepsilon_A, \varepsilon_Y)$, $\mathbb{F}_{U_A, U_Y}(U_A, U_Y)$ and $\mathbb{F}_{Z_A, Z_Y}(Z_A, Z_Y)$ are defined as below

$$\mathbb{F}_{\varepsilon_A, \varepsilon_Y}(\varepsilon_A, \varepsilon_Y) = \mathbb{C}(\mathbb{F}_{\varepsilon_A}(\varepsilon_A), \mathbb{F}_{\varepsilon_Y}(\varepsilon_Y)) \quad . \quad (2a)$$

$$\mathbb{F}_{U_A, U_Y}(U_A, U_Y) = \mathbb{C}(U_A, U_Y) \quad . \quad (2b)$$

$$\mathbb{F}_{Z_A, Z_Y}(Z_A, Z_Y) = \mathbb{C}(\Phi(Z_A), \Phi(Z_Y)) \quad . \quad (2c)$$

For the copula \mathbb{C} in Fig. 1b, the degree of association between U_A and U_Y may be quantified using measures of association such as Spearman's ρ_S [77, 78] or Kendall's τ_K [30] where $\rho_S, \tau_K \in [-1, +1]$. From the scale-invariance property of ρ_S and τ_K to the strictly increasing transformations $\mathbb{F}_{\varepsilon_A}$, $\mathbb{F}_{\varepsilon_Y}$, and Φ , the measure of association is the same between ε_A and ε_Y , between U_A and U_Y , and between Z_A and Z_Y , i.e., $\rho_S(\varepsilon_A, \varepsilon_Y) = \rho_S(U_A, U_Y) = \rho_S(Z_A, Z_Y) = \rho_{S\mathbb{C}}$. In other words, the orange, blue and red backdoor paths in Fig. 1a induce the same measure of non-causal association $\rho_{S\mathbb{C}}$ due to the copula \mathbb{C} . As discussed above, knowing the copula \mathbb{C} is necessary for identifying the causal effect of interest. The copula \mathbb{C} , although uniquely existing because of the continuous strictly increasing transformations $\mathbb{F}_{\varepsilon_A}$, $\mathbb{F}_{\varepsilon_Y}$, and Φ , is unknown and cannot be estimated from observational data because the noises are unobserved.

In principle, since the copula \mathbb{C} is unknown and unlearnable, it is inevitable to make assumptions about it to achieve causal effect identification. Specifically, \mathbb{C} may be chosen from any of the vast families of copulas such as Archimedean copulas [39] (Clayton, Frank, Gumbel, etc.), elliptical, or empirical copulas [5, 16, 48, 70]. In our current work, we limit our analysis by assuming and approximating the unknown copula $\mathbb{C}(U_A, U_Y)$ with one of the most well studied and used elliptical copula, namely the Gaussian copula. This copula has been used in the fields of quantitative finance [7, 41, 69], hydrology research [61, 92], logistics [35], astronomy [81], and similar fields [16, 48, 70]. The assumption and approximation of the unknown copula $\mathbb{C}(U_A, U_Y)$ with a Gaussian copula $\Phi_\rho(\Phi^{-1}(U_A), \Phi^{-1}(U_Y))$ in Eqs. (2a)-(2c) achieves the causal effect identification as the backdoor non-causal association

between Z_A and Z_Y may be identified as $\mathbb{F}_{Z_A, Z_Y}(Z_A, Z_Y) = \mathbb{C}(\Phi(Z_A), \Phi(Z_Y)) \cong \Phi_\rho(Z_A, Z_Y)$, where $\rho \in [-1, +1]$ is the Pearson's correlation between Z_A and Z_Y .

Unlike the noises Z_X that are assumed to be jointly Gaussian, the unobserved noises ε_X and U_X in Fig. 1a need not necessarily be linearly dependent. Hence, it may be more appropriate to equivalently represent the linear Pearson's correlation ρ in the Gaussian copula Φ_ρ in terms of the non-linear measure of association ρ_{Sc} (or τ_{Kc}) using the following results for bivariate Gaussian copula [34, 44].

$$\rho_{Sc} = \frac{6}{\pi} \arcsin\left(\frac{\rho}{2}\right), \quad \tau_{Kc} = \frac{2}{\pi} \arcsin(\rho), \quad \rho = 2 \sin\left(\frac{\pi \rho_{Sc}}{6}\right) = \sin\left(\frac{\pi \tau_{Kc}}{2}\right). \quad (3)$$

Therefore, the measure of backdoor non-causal association ρ_{Sc} due to the Gaussian copula assumption equates to the Gaussian copula parameter ρ as $\rho = 2 \sin(\pi \rho_{Sc} / 6)$ (i.e., $\rho_{Sc} \cong \rho$). For the Gaussian copula Φ_ρ assumption/approximation in Eq. (1d), the backdoor non-causal association $\rho_{Sc} \cong \rho$ is identifiable from Eq. (3), signifying that the SCM in Eq. (1d) and its causal effect are also identifiable, as well as learnable from an observational dataset $\{(A^\ell, Y^\ell)\}_{\ell=1}^{N_{train}}$ by rewriting it in terms of a parametric model as the proposed ρ -GNF in Fig. 1a (orange+blue+red) as below

$$\rho\text{-GNF} :: A := \mathbb{T}_A^{-1}(Z_A; \theta_A), \quad Y := \mathbb{T}_{Y|A}^{-1}(Z_Y; \theta_Y), \quad (Z_A, Z_Y) \sim \Phi_\rho(Z_A, Z_Y), \quad (4)$$

where $\mathbb{T}_A(\bullet; \theta_A)$ and $\mathbb{T}_{Y|A}(\bullet; \theta_Y)$ represent monotonic transformations parameterized by deep neural networks $\theta = (\theta_A, \theta_Y)$ using the integration-based (UMNN) transformer [87]. The conditioning of Y on its parent variable A in $\mathbb{T}_{Y|A}(\bullet; \theta_Y)$ is done with the graphical conditioner in GNF [88] as defined by the Directed Acyclic Graph (DAG) $A \rightarrow Y$ assumed in Fig. 1a. We aptly refer to our parametric model with the Gaussian copula assumption in Eq. (4) as ρ -GNF due to the similarities to GNF [88] that propose normalizing flow with UMNN monotonic transformer and graphical conditioner for only observational density estimation, and not for causal inference or sensitivity analysis (herein lies our novelty over GNF). The UMNN transformers and graphical conditioners are trained by maximizing the log-likelihood [33, 50, 88] of the observational training dataset $\{(A^\ell, Y^\ell)\}_{\ell=1}^{N_{train}}$ expressed as

$$\mathcal{L}(\theta_A, \theta_Y) = \sum_{\ell=1}^{N_{train}} \log(f_{A,Y}(A^\ell, Y^\ell)) = \sum_{\ell=1}^{N_{train}} \log\left(f_{A,Y}(\mathbb{T}_A^{-1}(Z_A^\ell; \theta_A), \mathbb{T}_{Y|A}^{-1}(Z_Y^\ell; \theta_Y))\right), \quad (5)$$

where $\mathbb{F}_{A,Y}(A^\ell, Y^\ell)$ denotes the joint probability density function (pdf) corresponding to the joint cumulative distribution function (CDF) $\mathbb{F}_{A,Y}(A^\ell, Y^\ell)$. The transformation of the base noise variables Z_A^ℓ and Z_Y^ℓ into random variables $A^\ell = \mathbb{T}_A^{-1}(Z_A^\ell; \theta_A)$ and $Y^\ell = \mathbb{T}_{Y|A}^{-1}(Z_Y^\ell; \theta_Y)$ from Eq. (4) implies that the joint pdf term $f_{A,Y}(A^\ell, Y^\ell)$ in Eq. (5) can be expressed in terms of the joint pdf $f_{Z_A, Z_Y}(Z_A^\ell, Z_Y^\ell) = \partial^2 \mathbb{F}_{Z_A, Z_Y}(Z_A^\ell, Z_Y^\ell) / \partial Z_A^\ell \partial Z_Y^\ell$ of the joint CDF $\mathbb{F}_{Z_A, Z_Y}(Z_A^\ell, Z_Y^\ell)$ as below

$$f_{A,Y}(A^\ell, Y^\ell) = f_{Z_A, Z_Y}(\mathbb{T}_A(A^\ell; \theta_A), \mathbb{T}_{Y|A}(Y^\ell; \theta_Y)) \left| \frac{\partial \mathbb{T}_A(A^\ell; \theta_A)}{\partial A^\ell} \frac{\partial \mathbb{T}_{Y|A}(Y^\ell; \theta_Y)}{\partial Y^\ell} \right|. \quad (6)$$

Hence, the assumption $\mathbb{F}_{Z_A, Z_Y}(Z_A, Z_Y) = \mathbb{C}(\Phi(Z_A), \Phi(Z_Y)) \cong \Phi_\rho(Z_A, Z_Y)$ achieves the primary aim/objective of sensitivity analysis by enabling the identification of the ACE since knowing the Gaussian joint distribution blocks the non-causal backdoor path. We note that the causal effect identification here comes at the cost of the normality assumption/approximation of the unobserved confounding (see Appendix 6 where we present the idea of replacing the Gaussian copula using any other suitable copulas). It further follows that the Gaussian copula [4, 7, 17, 29, 35, 37, 39, 44, 46, 61, 81, 89, 92, 93] assumption closely resembles the formulation of the computationally efficient and tractable density estimators, i.e., *normalizing flows* [3, 25, 31, 33, 49, 50, 62, 79, 80, 83] which are demonstrated to be universal density/distribution approximators [25] for monotonically increasing transformations such as UMNN transformers. It may be noted that, similar to normalizing flows, the Gaussian copula assumption facilitates efficient computation of Eqs. (5) and (6) due to *log-exp* cancellation resulting in a simple and tractable analytical expression for Eq. (5). Thus, enabling **computationally efficient training** of ρ -GNF in Eq. (4). The Gaussian copula assumption further enables sampling (Z_A, Z_Y) from $\mathbb{F}_{Z_A, Z_Y}(Z_A, Z_Y)$ efficiently for the estimation of Monte-Carlo expectation, thus enabling **computationally efficient inference**. Most importantly, the Gaussian copula assumption provides a single bounded sensitivity parameter $\rho \in [-1, +1]$ for sensitivity analysis that can be used to control/model/block/adjust the backdoor non-causal association under which the

ACE is identifiable. Thus, enabling **simple and efficient sensitivity analysis**. The ACE of interest identified from the ρ -GNF corresponding an assumed measure of non-causal association ρ is defined as

$$ACE_\rho = \mathbb{E}[Y_1 - Y_0] = \mathbb{E}_{\mathbb{P}(Y_1)}[Y_1] - \mathbb{E}_{\mathbb{P}(Y_0)}[Y_0] , \quad (7a)$$

$$\mathbb{P}(Y_a) = \mathbb{P}(Y|do(A := a)) = \sum_{Z_Y} \mathbb{P}(Y|a, Z_Y)\mathbb{P}(Z_Y) , \quad (7b)$$

where Y_a denotes the potential outcome under the intervention $A:=a$. In practise, the estimation of the ACE is done by Monte-Carlo expectation estimation by drawing the samples from the interventional distributions $\mathbb{P}(Y_1)$ and $\mathbb{P}(Y_0)$ to approximate $\mathbb{E}[Y_1]$ and $\mathbb{E}[Y_0]$, after having trained the ρ -GNF for a specific measure of unobserved confounding ρ on the given observational dataset. ‘*The First Law of Causal Inference*’ [52–54, 57] provides three steps to approximate $\mathbb{E}[Y_a]$ for an intervention $A:=a$.

(i) **Abduction:** N_s number of ρ -GNF noise-pairs $\{(Z_A^\ell, Z_Y^\ell)\}_{\ell=1}^{N_s}$ are sampled from the bivariate Gaussian distribution Φ_ρ with correlation ρ as defined in Eq. (4). (ii) **Action:** The structural equation corresponding to the treatment/interventional variable A in Eq. (4) is replaced with the desired interventional value $A:=a$ to obtain the mutilated ρ -GNF. (iii) **Prediction:** The potential outcome Y_a^ℓ for the ℓ^{th} sample is computed from Z_Y^ℓ and the mutilated ρ -GNF as

$$Y_a^\ell = \mathbb{T}_{Y|a}^{-1}(Z_Y^\ell; \theta_Y) \quad \forall \ell \in \{1, \dots, N_s\} \implies \mathbb{E}_{\mathbb{P}(Y_a)}[Y_a] \cong \frac{\sum_{\ell=1}^{N_s} Y_a^\ell}{N_s} . \quad (7c)$$

Similar to the E-value [85], we present ρ_{value} which represents the Gaussian copula parameter that explains away the causal association between the observed treatment A and the observed outcome Y . In other words, setting the Gaussian copula parameter $\rho = \rho_{value}$ results in $ACE_\rho = 0$, i.e., $\mathbb{E}_{\mathbb{P}(Y_1)}[Y_1] = \mathbb{E}_{\mathbb{P}(Y_0)}[Y_0]$, i.e., the potential outcomes are independent of the treatments/interventions. This implies that the strictly increasing transformation $\mathbb{T}_{Y|A}^{-1}$ modeling Y in Eq. (4) is independent of A , i.e., $Y = \mathbb{T}_Y^{-1}(Z_Y)$. From the scale-invariance property of Spearman’s correlation to strictly increasing transformations \mathbb{T}_A^{-1} and \mathbb{T}_Y^{-1} , we have $\rho_S(Z_A, Z_Y) = \rho_{Sc} = \rho_S(A, Y) = \rho_{S_{Obs}}$, where $\rho_{S_{Obs}}$ represents the observed Spearman’s correlation between the observational data A and Y . Thus, from Eq. (3), we have $\rho_{value} = 2 \sin(\pi \rho_{S_{Obs}} / 6)$. We experimentally verify and present the detailed results in Section 3. Hence, E-value and ρ_{value} represent different interpretations of the same concept.

Intuitively, for a given observational dataset over A and Y , the total observed association between A and Y as measured by, for instance, Spearman’s $\rho_S(A, Y)$ represents the combined effect due to both the causal ACE (via the frontdoor $A \rightarrow Y$, i.e., $\mathbb{T}_{Y|A}^{-1}$) and the non-causal ρ (via the backdoor $A \leftarrow Z_A \leftarrow \Phi_\rho \rightarrow Z_Y \rightarrow Y$, i.e., Φ_ρ) associations. Thus, we present the total observed association which is constant for a given observational dataset as a function of ρ and ACE_ρ that we refer as ρ_{curve} . This qualitative observation and reasoning may be interpreted as the conservation of the total observed association as a function of causal and non-causal association that is empirically validated in our experiments in Section 3 by plotting the ACE_ρ as a function of ρ . Note that even though, our ρ -GNF in Fig. 1a is originally formulated to perform sensitivity analysis in the presence of unobserved confounders from Fig. 1b, i.e., to address confounding bias, our ρ -GNF analysis equally applies to the bias analysis due to M bias [18] (also known as selection bias or collider bias, refer [18] for more details) from Fig. 1c. In other words, our ρ -GNF applies for the general application of bias analysis due to confounding and/or M bias (refer Appendix 5 for ρ -GNF generalization idea presentation).

In practise, the ρ_{curve} for a given observational dataset is obtained by varying the values of $\rho \in [-1, +1]$, i.e., we select $\rho = \{-0.99, -0.8, -0.6, -0.4, -0.2, 0.0, +0.2, +0.4, +0.6, +0.8, +0.99\}$ to train ρ -GNFs and compute the respective ACE_ρ from Eqs. (7a)-(7c) for every ρ -GNF to plot the ρ_{curve} as extrapolation of the points (ρ, ACE_ρ) as presented in Fig. 2 (synthetic dataset setting with continuous outcomes), Fig. 3 (synthetic dataset setting with binary outcomes) and Fig. 4 (real-world dataset setting with categorical outcomes denoting the total degree of child poverty ranging in 0-7 classes). The empirical ACE bounds are obtained as the infimum and supremum of the ρ_{curve} , i.e., $[\inf ACE_\rho, \sup ACE_\rho]$. Our empirical results in Section 3 show that the true ACE is bounded inside our empirical bounds from the ρ_{curve} with our bounds being narrower than the AF bounds [42, 64].

Table 1: Parameters α, β, δ of $SCM_{\alpha, \rho, \rho_{Obs}}$ from Eq. (8) with different causal association ($ACE_{\rho} = \alpha$), non-causal association ($\rho = \beta/\delta$) and total observed association ($\rho_{Obs} = \sigma_{A,Y}/\sigma_A\sigma_Y$).

$SCM_{\alpha, \rho, \rho_{Obs}}$	α (causal)	β	δ	ρ (non-causal)	ρ_{Obs} (total association)
$SCM_{0.2, -0.71, -0.55}$	0.2	-0.6	0.72	-0.71	-0.55
$SCM_{0.0, -0.55, -0.55}$	0.0	-0.4	0.52	-0.55	-0.55
$SCM_{-0.2, -0.32, -0.55}$	-0.2	-0.2	0.40	-0.32	-0.55
$SCM_{0.2, 0.32, 0.55}$	0.2	0.2	0.40	0.32	0.55
$SCM_{0.0, 0.55, 0.55}$	0.0	0.4	0.52	0.55	0.55
$SCM_{-0.2, 0.71, 0.55}$	-0.2	0.6	0.72	0.71	0.55

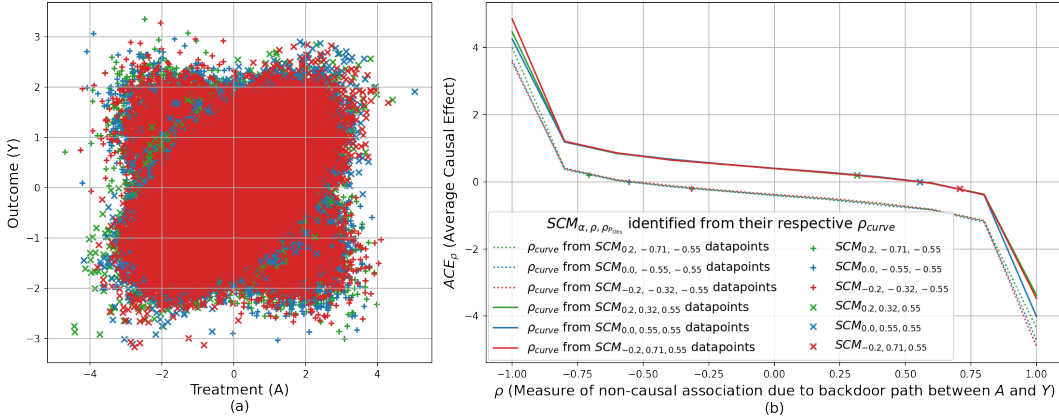


Figure 2: (a) Observational samples from the six SCMs in Table 1. (b) The ρ_{curve} obtained from the respective observational datasets by training ρ -GNFs.

3 Experimental Results, Analysis and Discussion

Our ρ -GNF with ‘*The First Law of Causal Inference*’ are implemented and published² by adapting the baseline code of GNF [88]³ and UMNN [87]⁴ to model the strictly increasing transformations used in ρ -GNF in PyTorch [51]. As normalizing flows are developed for continuous variables, we use the Gaussian dequantization trick from c-GNF [3] to model discrete variables into ρ -GNF. For the experiments, we present three different settings: (i) simulated dataset with continuous outcomes, (ii) simulated dataset with binary outcomes, and (iii) real-world dataset with categorical outcomes, i.e., the IMF (International Monetary Fund) program impact analysis on the degree of child poverty in the Global-South region consisting of 67 countries.

3.1 Simulated dataset with continuous outcomes

In our first set of simulated experiments, we perform sensitivity analysis using ρ -GNF and generate the ρ_{curve} for a given observational dataset thereby showing that, under the assumption of observed/assumed degree of confounding, the SCM and its causal effects are identifiable. Specifically, we consider the simple setting $SCM_{\alpha, \rho, \rho_{Obs}}$ from economics and econometrics [24] with continuous treatment A and outcome Y variables such that

$$SCM_{\alpha, \rho, \rho_{Obs}} :: A := \varepsilon_A, \quad Y := \alpha A + \varepsilon_Y, \quad \begin{bmatrix} \varepsilon_A \\ \varepsilon_Y \end{bmatrix} \sim N \left(\begin{bmatrix} 0 \\ 0 \end{bmatrix}, \begin{bmatrix} 1 & \beta \\ \beta & \delta \end{bmatrix} \right). \quad (8)$$

Fig. 2a shows the observational datapoints scatter plot of all the six SCMs from Table 1 with the observational distribution given as $\sigma_A^2 = 1$, $\sigma_Y^2 = \alpha^2 + \delta + 2\alpha\beta$, $\sigma_{A,Y} = \alpha + \beta$ and $\rho_{Obs} = \sigma_{A,Y}/\sigma_A\sigma_Y$.

²The ρ -GNF code in supplemental materials will also be published at <https://github.com/username/rhoGNF>

³<https://github.com/AWehenkel/Graphical-Normalizing-Flows>

⁴<https://github.com/AWehenkel/UMNN>

Even though the scatter plots are observationally equivalent, they are obtained from interventionally different SCMs/distributions due to different measure of non-causal association ρ and causal association $ACE_\rho=\alpha$ as presented in Table 1. We observe that the observationally equivalent SCMs have similar scatter plots as well as similar ρ_{curve} in Fig. 2b. Recall that the latter are obtained by training ρ -GNFs, hence the small discrepancies between them. Note that the points (ρ, ACE_ρ) on the ρ_{curve} for a given dataset corresponds to observationally equivalent but interventionally different SCMs. Thus, we also see that specific/unique interventionally different SCMs and their corresponding $ACE_\rho=\alpha$ are identifiable under the respectively assumed unobserved confounding $\rho=\beta/\delta$ as the point (ρ, ACE_ρ) on the ρ_{curve} . Observing the ρ_{curve} of a given observational dataset in Fig. 2b, the x-intercept point $(\rho_{value}, ACE_\rho=0)$ on the ρ_{curve} represents the measure of unobserved confounding, which we refer to as ρ_{value} , that actually explains away the causal effect/association, i.e., $ACE_\rho=0$. Setting $\rho=\rho_{value}=\rho_{P_{Obs}}$ in the ρ -GNF implies that $\rho_S(Z_A, Z_Y)=\rho_S(A, Y)=\rho_{S_{Obs}}$ such that $T_{Y|A}^{-1}$ is required to be independent of A , which results in $ACE_\rho=0$, i.e., the causal effect is explained away. Thus, we note that E-value [85] and ρ_{value} represent different versions of the same concept. Similar to the E-value that can be computed directly from the observational dataset [43], the ρ_{value} is also identified as a single, bounded intuitive parameter that can be computed directly from Spearman’s rho $\rho_{S_{Obs}}$ between the observed treatment A and the outcome Y , i.e., $\rho_{value}=2 \sin(\pi \rho_{S_{Obs}}/6)$. This further shows the similarities between the concepts of E-value and ρ_{value} .

The ρ_{value} equips an analyst/domain-expert to determine the sign of the ACE (i.e., whether the treatment is harmful or beneficial), which is arguably the most important part of the ACE and one of the ultimate goals of causal inference. Specifically, suppose the domain expert hypothesizes a measure of confounding in the interval $[\rho_{min}, \rho_{max}]$. Then, the ρ_{curve} enables us to bound the true ACE to the narrower interval $[ACE_{\rho_{max}}, ACE_{\rho_{min}}]$, which may in turn help us identify the most important insight of the causal inference, i.e., the sign of the true ACE. In particular, if $\rho_{min} > \rho_{value}$ (or $\rho_{max} < \rho_{value}$) then we may conclude that the true ACE is positive (or negative), as observed in the ρ_{curve} in Fig. 2b. This identification of the sign of the ACE is typically not possible with the AF bounds, as they are typically too wide and include positive/zero/negative values.

We observe that the SCM in Eq. (8) used to demonstrate ρ -GNF with continuous outcomes may be considered as simple case of linear SCM as studied in [8]. However, as the ρ -GNF is parameterized to learn arbitrary non-linear functions using UMNN transformers [87], our work may be viewed as the generalization of the sensitivity analysis of simple linear SCM [8] to complex non-linear SCM as presented in the subsequent experiments in non-linear settings with binary and categorical outcomes.

3.2 Simulated dataset with binary outcomes

In the second set of experiments, we consider multiple randomly generated observational datasets from randomly sampled data generating processes as in [58, 73, 75], where all variables are binary. As proposed in [58, 73, 75], we randomly sample the Bernoulli parameters $\{\mathbb{P}(U), \mathbb{P}(A|U), \mathbb{P}(Y|A, U)\}$ of the data generating process (DGP) from the uniform distribution in $[0, 1]$, where U denotes the confounder of A and Y which is intentionally hidden during training to simulate the unobserved confounding. For this simple binary outcome/treatment/confounder case, the AF bounds with a constant width of 1 ($= p_1+p_0$) are presented in [15, 42, 64, 75] as the gold-standard of bounds with 100% certainty of including the true ACE as

$$AF_{lower}=q_1p_1-q_0p_0-p_1 \leq ACE_{true} \leq AF_{upper}=q_1p_1-q_0p_0+p_0 \quad (9)$$

where $p_a=\mathbb{P}(A=a)$ and $q_a=\mathbb{P}(Y=1|A=a)$ are estimated using observational data. In Fig. 3, we see that the ρ_{curve} does include the true ACE in all of the twenty randomly generated DGPs. Further, we obtain a narrower bound of 0.83 ± 0.03 (i.e., $\approx 14\%$ narrower than the AF bounds) such that our empirical bounds lie within the AF bounds, unlike VW bounds which may be wider than the AF bounds as shown in [73]. The former comes as no surprise: Since our bounds are empirically obtained particularly assuming the Gaussian copula, they must lie within the AF bounds. This may be verified from Fig. 3, i.e., $AF_{lower} \leq \inf ACE_\rho \leq ACE_{true} \leq \sup ACE_\rho \leq AF_{upper}$.

3.3 Real-world IMF program impact analysis on child poverty with categorical outcomes

A recent study analyzing the impact of the IMF program on the degree of child poverty [2] using a large-scale real-world dataset [11–14, 23] considers adjusting/controlling for several micro- and macro-economic confounders such as political-will, economy, polity, and public spending, and present

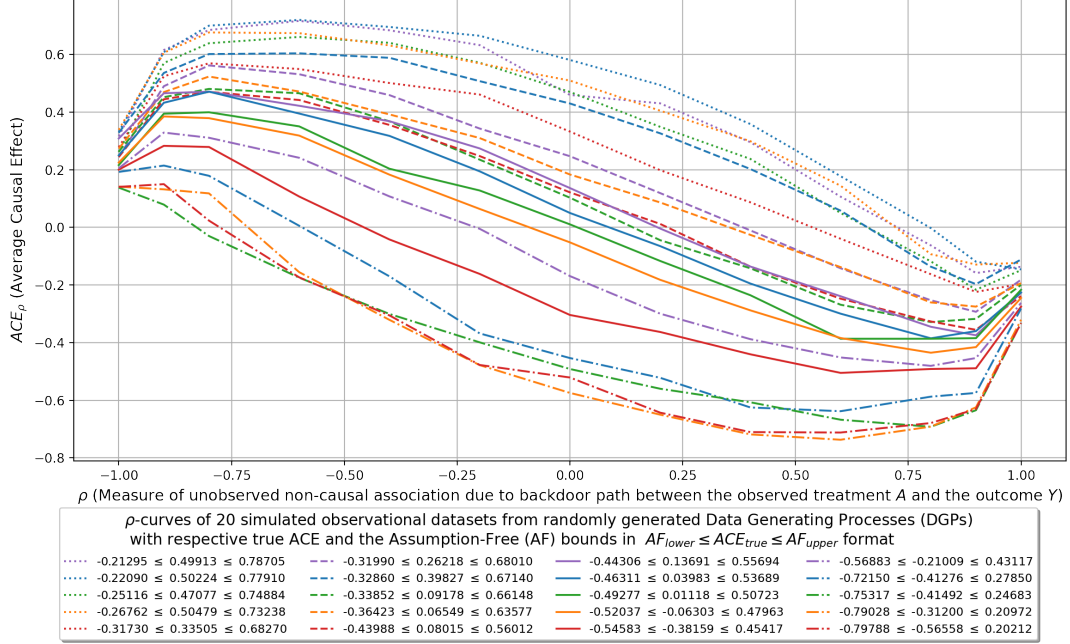


Figure 3: Twenty ρ_{curves} each corresponding to a randomly generated dataset from a randomly parameterized DGP. The legend of each ρ_{curve} presents the true ACE identified using *do*-calculus as well as the AF bounds from Eq. (9) identified from the DGP parameters. We observe that the true ACE is indeed included for all the ρ_{curve} with our bounds narrower than the AF bounds.

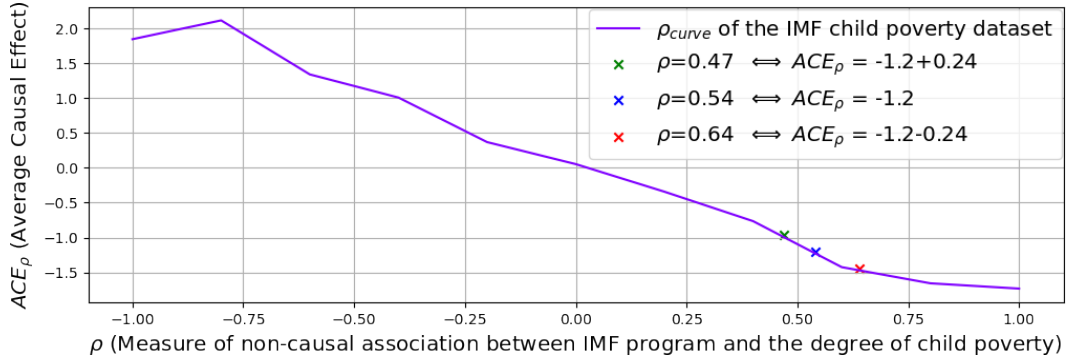


Figure 4: ρ_{curve} generated for the categorical outcome, i.e., total degree of the child poverty in the IMF child poverty dataset.

an ACE estimate of -1.2 ± 0.24 . From the ρ_{curve} in Fig. 4, we see that the ACE estimate interval of -1.2 ± 0.24 corresponds to $\rho = [0.47, 0.64]$, i.e., a significant measure of non-causal association is required to explain away the ACE. Since the outcome, i.e., the total degree of child poverty is categorical, unlike binary outcomes, the theoretical AF bounds are not available. However, the adaptability of ρ -GNF for both discrete and continuous outcome facilitates the identification of our empirical bounds from the ρ_{curve} in Fig. 4, helping the analyst/domain-expert to make inference based on the sensitivity analysis.

From Fig. 4, we see that the $\rho_{value} \cong 0$. Thus, for $\rho > 0$ we have $ACE_{\rho} < 0$, i.e., if the analyst believes that the non-causal association due unobserved confounding between the IMF program selection and the child poverty is positive, then it may be concluded that the IMF program has a beneficial impact in the reduction of child poverty as the ACE is negative. It is not far-fetching to reason that the confounding association has to be positive because a country with severe socioeconomic turmoil ($Z_Y \uparrow$) causing severe child poverty has higher incentives to apply for the IMF program ($Z_A \uparrow$) to overcome the socioeconomic turmoil. Similarly, a country in least socioeconomic turmoil ($Z_Y \downarrow$) has

less incentives to apply for the IMF program ($Z_A \downarrow$). Hence, from the reasoning of positively correlated non-causal backdoor noises ($Z_A \uparrow \Leftrightarrow Z_Y \uparrow$ or $Z_A \downarrow \Leftrightarrow Z_Y \downarrow$) and $\rho_{value} \cong 0$ from Fig. 4, we reaffirm the beneficial nature of the IMF program in the reduction of child poverty as presented in [2]. Effectively, instead of the uninformative widest bounds width of 7 (refer Appendix 7.1), we obtain a narrower width of 1.7 of only positive ACE, i.e., a bounds reduction of 75.7% which is extremely informative.

4 Conclusion

We proposed a novel approach for sensitivity analysis termed ρ -GNF to bound the causal effect in the risk difference scale where $\rho \in [-1, +1]$ is a bounded sensitivity parameter representing the unobserved backdoor non-causal association between the treatment and outcome due to the unobserved confounding modeled using the most well studied and widely popular Gaussian copula. We showed that ρ -GNF enabled us to estimate the causal effect as a function of ρ in the form of ρ_{curve} . Under the Gaussian copula assumption, the ρ_{curve} enabled us to identify narrower empirical bounds in contrast to the wider AF and VW bounds, irrespective of discrete or continuous variables. We identified ρ_{value} as the measure of the unobserved confounding that explains away the causal effect and presented the conceptual similarities to the widely popular E-value. Further, the ρ_{curve} enabled us to provide finer bounds for the causal effect given an interval of ρ values that the domain expert considers appropriate or realistic to be able to identify arguably the most important part of the causal effect, i.e., the sign of the ACE, thus facilitating in inferring if the treatment is beneficial or harmful. In summary, ρ -GNF offers an alternative way to inject domain knowledge in the form of a copula to provide sharp and narrow empirical ACE bounds as well as additional insights on the sign of the ACE from the observation of the ρ_{curve} and ρ_{value} .

References

- [1] ANGRIST, J. D., IMBENS, G. W., AND RUBIN, D. B. Identification of causal effects using instrumental variables. *Journal of the American Statistical Association (JASA)* 91, 434 (1996), 444–455.
- [2] BALGI, S., PEÑA, J. M., AND DAOUD, A. Counterfactual analysis of the impact of the imf program on child poverty in the global-south region using causal-graphical normalizing flows. *arXiv preprint arXiv:2202.09391* (2022).
- [3] BALGI, S., PEÑA, J. M., AND DAOUD, A. Personalized public policy analysis in social sciences using causal-graphical normalizing flows. In *AAAI conference on Artificial Intelligence (AAAI)* (2022).
- [4] BECKER, J.-M., PROKSCH, D., AND RINGLE, C. M. Revisiting gaussian copulas to handle endogenous regressors. *Journal of the Academy of Marketing Science (JAMS)* 50, 1 (2022), 46–66.
- [5] BENALI, F., BODÉNÈS, D., LABROCHE, N., AND DE RUNZ, C. MTCopula: Synthetic complex data generation using copula. In *International Workshop on Design, Optimization, Languages and Analytical Processing of Big Data (DOLAP)* (2021), pp. 51–60.
- [6] BRUMBACK, B. A., HERNÁN, M. A., HANEUSE, S. J., AND ROBINS, J. M. Sensitivity analyses for unmeasured confounding assuming a marginal structural model for repeated measures. *Statistics in Medicine* 23, 5 (2004), 749–767.
- [7] CHERUBINI, U., LUCIANO, E., AND VECCHIATO, W. *Copula methods in finance*. John Wiley & Sons, 2004.
- [8] CINELLI, C., KUMOR, D., CHEN, B., PEARL, J., AND BAREINBOIM, E. Sensitivity analysis of linear structural causal models. In *International Conference on Machine Learning (ICML)* (2019), vol. 97, pp. 1252–1261.
- [9] COCHRAN, W. G., AND RUBIN, D. B. Controlling bias in observational studies: A review. *Sankhyā: The Indian Journal of Statistics, Series A* (1973), 417–446.
- [10] CORNFIELD, J., HAENSZEL, W., HAMMOND, E. C., LILIENFELD, A. M., SHIMKIN, M. B., AND WYNDER, E. L. Smoking and lung cancer: Recent evidence and a discussion of some questions. *Journal of the National Cancer Institute* 22, 1 (1959), 173–203.
- [11] DAOUD, A., AND JOHANSSON, F. Estimating treatment heterogeneity of international monetary fund programs on child poverty with generalized random forest. *SocArXiv* (2019).
- [12] DAOUD, A., NOSRATI, E., REINSBERG, B., KENTIKELIS, A. E., STUBBS, T. H., AND KING, L. P. Impact of international monetary fund programs on child health. *Proceedings of the National Academy of Sciences (PNAS)* 114, 25 (2017), 6492–6497.
- [13] DAOUD, A., AND REINSBERG, B. Structural adjustment, state capacity and child health: Evidence from IMF programmes. *Epidemiology* 48, 2 (2018), 445–454.
- [14] DAOUD, A., REINSBERG, B., KENTIKELIS, A. E., STUBBS, T. H., AND KING, L. P. The international monetary fund’s interventions in food and agriculture: An analysis of loans and conditions. *Food Policy* 83 (2019), 204–218.
- [15] DING, P., AND VANDERWEELE, T. J. Sensitivity analysis without assumptions. *Epidemiology (Cambridge, Mass.)* 27, 3 (2016), 368.
- [16] DURANTE, F., AND SEMPI, C. *Principles of copula theory*. CRC press Boca Raton, 2016.
- [17] ELIDAN, G. Copula bayesian networks. *Neural Information Processing Systems (NeurIPS)* 23 (2010).
- [18] ELWERT, F., AND WINSHIP, C. Endogenous selection bias: The problem of conditioning on a collider variable. *Annual Review of Sociology* 40 (2014), 31–53.
- [19] FIENBERG, S., AND DUNCAN, O. D. Introduction to structural equation models. *Journal of the American Statistical Association (JASA)* 72 (1975), 485.
- [20] FISHER, R. A. Design of experiments. *British Medical Journal (BMJ)* 1 (1936), 554–554.
- [21] GOLDBERGER, A. S. Structural equation methods in the social sciences. *Econometrica* 40 (1972), 979–1001.

- [22] HAAVELMO, T. The statistical implications of a system of simultaneous equations. *Econometrica* 11 (1943), 1–12.
- [23] HALLERÖD, B., ROTHSTEIN, B., DAOUD, A., AND NANDY, S. Bad governance and poor children: A comparative analysis of government efficiency and severe child deprivation in 68 low-and middle-income countries. *World Development* 48 (2013), 19–31.
- [24] HOOVER, K. D. Causality in economics and econometrics. *SSRN eLibrary* (2006).
- [25] HUANG, C., KRUEGER, D., LACOSTE, A., AND COURVILLE, A. C. Neural autoregressive flows. In *International Conference on Machine Learning (ICML)* (2018), pp. 2083–2092.
- [26] HUANG, Y., AND VALTORTA, M. Pearl’s calculus of intervention is complete. In *Uncertainty in Artificial Intelligence (UAI)* (2006).
- [27] IMBENS, G. W. Sensitivity to exogeneity assumptions in program evaluation. *American Economic Review* 93, 2 (2003), 126–132.
- [28] IMBENS, G. W., AND ANGRIST, J. D. Identification and estimation of local average treatment effects. *Econometrica* 62, 2 (1994), 467–475.
- [29] KAMTHE, S., ASSEFA, S. A., AND DEISENROTH, M. P. Copula flows for synthetic data generation. *ArXiv abs/2101.00598* (2021).
- [30] KENDALL, M. G. A new measure of rank correlation. *Biometrika* 30, 1/2 (1938), 81–93.
- [31] KHEMAKHEM, I., MONTI, R., LEECH, R., AND HYVARINEN, A. Causal autoregressive flows. In *International Conference on Artificial Intelligence and Statistics (AISTATS)* (2021), pp. 3520–3528.
- [32] KING, M. A. S. Goldberger and O. D. Duncan. Structural equation models in the social sciences. *The Economic Journal* 84 (1974), 212–214.
- [33] KOBYZEV, I., PRINCE, S., AND BRUBAKER, M. Normalizing flows: An introduction and review of current methods. *IEEE Transactions on Pattern Analysis and Machine Intelligence (TPAMI)* (2020), 1–1.
- [34] KRUSKAL, W. H. Ordinal measures of association. *Journal of the American Statistical Association (JASA)* 53, 284 (1958), 814–861.
- [35] KUMAR, P. Copula functions and applications in engineering. In *Logistics, supply chain and financial predictive analytics*. Springer, 2019, pp. 195–209.
- [36] LASH, T. L., FOX, M. P., FINK, A. K., ET AL. *Applying quantitative bias analysis to epidemiologic data*, vol. 533. Springer, 2009.
- [37] LASZKIEWICZ, M., LEDERER, J., AND FISCHER, A. Copula-based normalizing flows. In *ICML Workshop on Invertible Neural Networks, Normalizing Flows, and Explicit Likelihood Models* (2021).
- [38] LASZKIEWICZ, M., LEDERER, J., AND FISCHER, A. Marginal tail-adaptive normalizing flows, 2022.
- [39] LING, C. K., FANG, F., AND KOLTER, J. Z. Deep archimedean copulas. *Neural Information Processing Systems (NeurIPS)* 33 (2020), 1535–1545.
- [40] LOSHCHILOV, I., AND HUTTER, F. Decoupled weight decay regularization. In *International Conference on Learning Representations (ICLR)* (2019).
- [41] MACKENZIE, D., AND SPEARS, T. The formula that killed wall street: The gaussian copula and modelling practices in investment banking. *Social Studies of Science* 44, 3 (2014), 393–417.
- [42] MANSKI, C. F. Nonparametric bounds on treatment effects. *American Economic Review* 80, 2 (1990), 319–323.
- [43] MATHUR, M. B., DING, P., RIDDELL, C. A., AND VANDERWEELE, T. J. Website and R package for computing E-values. *Epidemiology* 29, 5 (2018), e45.
- [44] MEYER, C. The bivariate normal copula. *Communications in Statistics-Theory and Methods* 42, 13 (2013), 2402–2422.
- [45] MOOIJ, J. M., PETERS, J., JANZING, D., ZSCHEISCHLER, J., AND SCHÖLKOPF, B. Distinguishing cause from effect using observational data: Methods and benchmarks. *Journal of Machine Learning Research (JMLR)* 17, 1 (2016), 1103–1204.

- [46] NAGLER, T., AND VATTER, T. Solving estimating equations with copulas. *arXiv preprint arXiv:1801.10576* (2018).
- [47] NEAL, B. Introduction to causal inference from a machine learning perspective. *Course Lecture Notes (draft)* (2020).
- [48] NELSEN, R. B. *An introduction to copulas*. Springer Science & Business Media, 2007.
- [49] PAPAMAKARIOS, G., MURRAY, I., AND PAVLAKOU, T. Masked autoregressive flow for density estimation. In *Neural Information Processing Systems (NeurIPS)* (2017), pp. 2338–2347.
- [50] PAPAMAKARIOS, G., NALISNICK, E., REZENDE, D. J., MOHAMED, S., AND LAKSHMINARAYANAN, B. Normalizing flows for probabilistic modeling and inference. *Journal of Machine Learning Research (JMLR)* 22, 57 (2021), 1–64.
- [51] PASZKE, A., GROSS, S., CHINTALA, S., CHANAN, G., YANG, E., DEVITO, Z., LIN, Z., DESMAISON, A., ANTIGA, L., AND LERER, A. Automatic Differentiation in PyTorch. *NeurIPS Workshops* (2017).
- [52] PEARL, J. Probabilities of causation: Three counterfactual interpretations and their identification. *Synthese* 121, 1 (1999), 93–149.
- [53] PEARL, J. Causal inference in statistics: An overview. *Statistics Surveys* 3 (2009), 96–146.
- [54] PEARL, J. *Causality: Models, reasoning and inference*. Cambridge University Press, USA, 2009.
- [55] PEARL, J. The *do*-calculus revisited. In *Uncertainty in Artificial Intelligence (UAI)* (2012), p. 3–11.
- [56] PEARL, J. Interpretation and identification of causal mediation. *Psychological methods* 19, 4 (2014), 459.
- [57] PEARL, J., AND MACKENZIE, D. *The Book of Why: The New Science of Cause and Effect*, 1st ed. Basic Books, Inc., USA, 2018.
- [58] PEÑA, J. M. Simple yet sharp sensitivity analysis for unmeasured confounding. *Journal of Causal Inference (JCI)* 10, 1 (2022), 1–17.
- [59] PETERS, J., JANZING, D., AND SCHÖLKOPF, B. *Elements of causal inference: Foundations and learning algorithms*. The MIT Press, 2017.
- [60] PLOCH, D. R., GOLDBERGER, A. S., AND DUNCAN, O. D. Structural equations models in the social sciences. *Social Forces* 54 (1975), 503.
- [61] RENARD, B., AND LANG, M. Use of a gaussian copula for multivariate extreme value analysis: Some case studies in hydrology. *Advances in Water Resources* 30, 4 (2007), 897–912.
- [62] REZENDE, D., AND MOHAMED, S. Variational inference with normalizing flows. In *International Conference on Machine Learning (ICML)* (2015), pp. 1530–1538.
- [63] ROBINS, J. M. A new approach to causal inference in mortality studies with a sustained exposure period—application to control of the healthy worker survivor effect. *Mathematical Modelling* 7, 9 (1986), 1393–1512.
- [64] ROBINS, J. M. The analysis of randomized and non-randomized aids treatment trials using a new approach to causal inference in longitudinal studies. *Health Service Research Methodology: A Focus on AIDS* (1989), 113–159.
- [65] ROBINS, J. M., AND GREENLAND, S. Identifiability and exchangeability for direct and indirect effects. *Epidemiology* (1992), 143–155.
- [66] ROBINS, J. M., AND HERNÁN, M. A. Estimation of the causal effects of time-varying exposure. *Longitudinal Data Analysis (LDA)* (2008), 553–599.
- [67] ROTHMAN, K. J., GREENLAND, S., LASH, T. L., ET AL. *Modern epidemiology*, vol. 3. Wolters Kluwer Health/Lippincott Williams & Wilkins Philadelphia, 2008.
- [68] RUBIN, D. B. Formal mode of statistical inference for causal effects. *Journal of Statistical Planning and Inference (JSPI)* 25, 3 (1990), 279–292.
- [69] SALMON, F. Recipe for disaster: The formula that killed wall street. *Wired Magazine* 17, 3 (2009), 17–03.
- [70] SALVADORI, G., DE MICHELE, C., KOTTEGODA, N. T., AND ROSSO, R. *Extremes in nature: An approach using copulas*, vol. 56. Springer Science & Business Media, 2007.

- [71] SCHLESSELMAN, J. J. Assessing effects of confounding variables. *American Journal of Epidemiology* 108, 1 (1978), 3–8.
- [72] SHPITSER, I., AND PEARL, J. Identification of joint interventional distributions in recursive semi-markovian causal models. In *AAAI conference on Artificial Intelligence (AAAI)* (2006), pp. 1219–1226.
- [73] SJÖLANDER, A. A note on a sensitivity analysis for unmeasured confounding, and the related E-value. *Journal of Causal Inference (JCI)* 8, 1 (2020), 229–248.
- [74] SJÖLANDER, A., AND GREENLAND, S. Are E-values too optimistic or too pessimistic? both and neither! *International Journal of Epidemiology* (2022).
- [75] SJÖLANDER, A., AND HÖSSJER, O. Novel bounds for causal effects based on sensitivity parameters on the risk difference scale. *Journal of Causal Inference (JCI)* 9, 1 (2021), 190–210.
- [76] SKLAR, A. Fonctions de répartition à n dimensions et leurs marges. *Publ. inst. statist. univ. Paris* 8 (1959), 229–231.
- [77] SPEARMAN, C. The proof and measurement of association between two things. *The American Journal of Psychology* 100, 3/4 (1987), 441–471.
- [78] SPEARMAN, C. The proof and measurement of association between two things. *International Journal of Epidemiology* 39, 5 (2010), 1137–1150.
- [79] TABAK, E., AND TURNER, C. A family of nonparametric density estimation algorithms. *Communications on Pure and Applied Mathematics* 66 (2013), 145–164.
- [80] TABAK, E., AND VANDEN-EIJNDEN, E. Density estimation by dual ascent of the log-likelihood. *Communications in Mathematical Sciences* 8 (2010), 217–233.
- [81] TAKEUCHI, T. T. Constructing a bivariate distribution function with given marginals and correlation: Application to the galaxy luminosity function. *Monthly Notices of the Royal Astronomical Society* 406, 3 (2010), 1830–1840.
- [82] TIAN, J., AND PEARL, J. A general identification condition for causal effects. In *AAAI conference on Artificial Intelligence (AAAI)* (2002), p. 567–573.
- [83] URIA, B., MURRAY, I., AND LAROCHELLE, H. RNADE: The real-valued neural autoregressive density-estimator. In *Neural Information Processing Systems (NeurIPS)* (2013), pp. 2175–2183.
- [84] VANDERWEELE, T. J., AND ARAH, O. A. Bias formulas for sensitivity analysis of unmeasured confounding for general outcomes, treatments, and confounders. *Epidemiology* (2011), 42–52.
- [85] VANDERWEELE, T. J., AND DING, P. Sensitivity analysis in observational research: Introducing the E-value. *Annals of Internal Medicine* 167, 4 (2017), 268–274.
- [86] VEITCH, V., AND ZAVERI, A. Sense and sensitivity analysis: Simple post-hoc analysis of bias due to unobserved confounding. *Neural Information Processing Systems (NeurIPS)* 33 (2020), 10999–11009.
- [87] WEHENKEL, A., AND LOUPPE, G. Unconstrained monotonic neural networks. In *Neural Information Processing Systems (NeurIPS)* (2019), pp. 1545–1555.
- [88] WEHENKEL, A., AND LOUPPE, G. Graphical normalizing flows. In *International Conference on Artificial Intelligence and Statistics (AISTATS)* (2021), pp. 37–45.
- [89] WIESE, M., KNOBLOCH, R., AND KORN, R. Copula & marginal flows: Disentangling the marginal from its joint. *ArXiv abs/1907.03361* (2019).
- [90] WRIGHT, S. Correlation and causation. *Journal of Agricultural Research (JAR)* 20 (1921), 557–585.
- [91] YANG, J., CHENG, S., AND ZHANG, L. Bivariate copula decomposition in terms of comonotonicity, countermonotonicity and independence. *Insurance: Mathematics and Economics* 39, 2 (2006), 267–284.
- [92] ZHANG, L., AND SINGH, V. P. *Copulas and their applications in water resources engineering*. Cambridge University Press, 2019.
- [93] ZHAO, Y., AND UDELL, M. Missing value imputation for mixed data via gaussian copula. In *ACM Special Interest Group on Knowledge Discovery and Data Mining (SIGKDD)* (2020), pp. 636–646.
- [94] ZHENG, Y., YANG, J., AND HUANG, J. Z. Approximation of bivariate copulas by patched bivariate fréchet copulas. *Insurance: Mathematics and Economics* 48, 2 (2011), 246–256.

5 CAREFL and c-GNF as particular cases of ρ -GNF with $\rho=0$, i.e., unconfoundedness assumption of A and Y

Recently, Causal Autoregressive Flow (CAREFL) [31] and Causal-Graphical Normalizing Flow (c-GNF) [3] proposed normalizing flows for the identification and estimation of the causal effects under the assumption of unconfoundedness and multi-variate standard normal distribution with zero mean and identity covariance matrix. For differences in CAREFL and c-GNF, we refer c-GNF [3]. Setting $\rho=0$ in ρ -GNF actually corresponds to identity covariance matrix such that the joint distribution $\mathbb{F}_{Z_A, Z_Y}(Z_A, Z_Y) = \Phi_0(Z_A, Z_Y) = \Phi(Z_A)\Phi(Z_Y)$, which implies the noises Z_A and Z_Y are independent, i.e., the treatment A and the outcome Y satisfy the necessary assumption of unconfoundedness assumption for the identification of causal effects following the completeness result of *do*-calculus [26, 55, 72, 82], enabling CAREFL and c-GNF to perform causal effect identification and estimation. The c-GNF even goes beyond the average causal effect and into the individual causal effect (ICE) to identify personalized optimal treatments by using ‘*The First Law of Causal Inference*’. In conclusion, CAREFL and c-GNF may be viewed as particular $\rho=0$ instantiations of ρ -GNF, i.e., the y-intercept point $(0, ACE)$ from the ρ_{curve} represents the CAREFL and c-GNF.

6 Relaxing the assumption of Gaussian copula in ρ -GNF to define Copula SCM

Let $\mathbb{I}=[0, 1]$. A 2-Copula \mathbb{C} is defined (from [48]) as a bivariate function $\mathbb{C} : \mathbb{I}^2 \rightarrow \mathbb{I}$ such that:

1. (uniform marginals) for all $U_A, U_Y \in \mathbb{I}$,

$$\mathbb{C}(U_A, 0)=0, \quad \mathbb{C}(U_A, 1)=U_A, \quad \mathbb{C}(0, U_Y)=0, \quad \mathbb{C}(1, U_Y)=U_Y \quad (10a)$$

2. (2-increasing) for all $U_A^1, U_Y^1, U_A^2, U_Y^2 \in \mathbb{I}$ such that $U_A^1 \leq U_A^2$ and $U_Y^1 \leq U_Y^2$,

$$\mathbb{C}(U_A^2, U_Y^2) - \mathbb{C}(U_A^2, U_Y^1) + \mathbb{C}(U_A^1, U_Y^1) - \mathbb{C}(U_A^1, U_Y^2) \geq 0. \quad (10b)$$

The objective of the copula, as the name suggests, is to ‘*tie*’ or ‘*link*’ or ‘*couple*’ the dependence between U_A and U_Y . It follows from Sklar’s theorem [76] that any joint distribution \mathbb{F}_{U_A, U_Y} can be represented with the help of copula as below.

Theorem 6.1 (Sklar’s theorem [76]) *Let \mathbb{F}_{U_A, U_Y} be a joint distribution function with uniform marginals in \mathbb{I} . Then there exists a copula \mathbb{C} such that for all $U_A, U_Y \in \mathbb{I}$,*

$$\mathbb{F}_{U_A, U_Y}(U_A, U_Y) = \mathbb{C}(U_A, U_Y) \quad (11a)$$

$$\mathbb{F}_{\varepsilon_A, \varepsilon_Y}(\varepsilon_A, \varepsilon_Y) = \mathbb{C}(\mathbb{F}_{\varepsilon_A}(\varepsilon_A), \mathbb{F}_{\varepsilon_Y}(\varepsilon_Y)) \quad (11b)$$

$$\mathbb{F}_{Z_A, Z_Y}(Z_A, Z_Y) = \mathbb{C}(\Phi(Z_A), \Phi(Z_Y)) \quad (11c)$$

Eqs. (11b) and (11c) follow from the scale-invariance property of copula \mathbb{C} to strictly increasing transformations (CDFs) $\mathbb{F}_{\varepsilon_A}, \mathbb{F}_{\varepsilon_Y}$ and Φ . In particular the approximation of the joint distribution $\mathbb{F}_{Z_A, Z_Y}(Z_A, Z_Y)$ to Gaussian joint distribution $\Phi_\rho(Z_A, Z_Y) = \Phi_\rho$ resulting in ρ -GNF corresponds to the copula \mathbb{C} assumed as a Gaussian copula $\mathbb{C}(U_A, U_Y) = \Phi_\rho(\Phi^{-1}(U_A), \Phi^{-1}(U_Y))$ [44]. The assumption of approximating $\mathbb{F}_{Z_A, Z_Y}(Z_A, Z_Y)$ with a Gaussian copula $\mathbb{C}(U_A, U_Y) = \Phi_\rho(\Phi^{-1}(U_A), \Phi^{-1}(U_Y))$ is made in such a way as to facilitate the following benefits: **Constraint (i) - Computationally efficient training**, **Constraint (ii) - Computationally efficient inference**, **Constraint (iii) - Bounded sensitivity parameter representing the measure of non-causal backdoor association**.

However, in principle, the ρ -GNF may be extended to accommodate any desired copula $\mathbb{C}(U_A, U_Y)$ other than the assumed Gaussian copula while maintaining the other parts with strictly increasing transformations parameterized by UMNN transformer [87] in the following manner.

$$SCM_{\mathbb{C}} :: A := \mathbb{F}_A^{-1}(U_A) = \mathbb{T}_A^{-1}(U_A; \theta_A), \quad Y := \mathbb{F}_{Y|A}^{-1}(U_Y) = \mathbb{T}_{Y|A}^{-1}(U_Y; \theta_Y), \quad (12a)$$

$$(U_A, U_Y) \sim \mathbb{C}(U_A, U_Y), \quad (12b)$$

where $\mathbb{T}_A(\bullet; \theta_A)$ and $\mathbb{T}_{Y|A}(\bullet; \theta_Y)$ represent the strictly increasing transformations parameterized by deep neural networks $\theta = (\theta_A, \theta_Y)$ using the integration-based Unconstrained Monotonic Neural

Network (UMNN) transformer [87]. The UMNN transformers parameterized by deep neural networks θ are trained by maximizing the log-likelihood of the observational training dataset $\{(A^\ell, Y^\ell)\}_{\ell=1}^{N_{train}}$ expressed as

$$\mathcal{L}(\theta_A, \theta_Y) = \sum_{\ell=1}^{N_{train}} \log(f_{A,Y}(A^\ell, Y^\ell)) = \sum_{\ell=1}^{N_{train}} \log\left(f_{A,Y}(\mathbb{T}_A^{-1}(U_A^\ell; \theta_A), \mathbb{T}_{Y|A^\ell}^{-1}(U_Y^\ell; \theta_Y))\right) \quad (13)$$

where $\mathbb{F}_{A,Y}(A^\ell, Y^\ell)$ denotes the joint probability density function (pdf) corresponding to the joint cumulative distribution function $\mathbb{F}_{A,Y}(A^\ell, Y^\ell)$. As we can express $A^\ell = \mathbb{T}_A^{-1}(U_A^\ell; \theta_A)$ and $Y^\ell = \mathbb{T}_{Y|A^\ell}^{-1}(U_Y^\ell; \theta_Y)$ from Eq. (12a), using the transformation of the base uniform variables U_A^ℓ, U_Y^ℓ into random variables A^ℓ, Y^ℓ , the joint pdf term $\mathbb{F}_{A,Y}(A^\ell, Y^\ell)$ in Eq. (13) can be expressed in terms of the joint pdf $\mathbb{F}_{U_A, U_Y}(U_A^\ell, U_Y^\ell)$ corresponding to the joint distribution $\mathbb{F}_{U_A, U_Y}(U_A^\ell, U_Y^\ell)$ as below

$$f_{A,Y}(A^\ell, Y^\ell) = f_{U_A, U_Y}(\mathbb{T}_A(A^\ell; \theta_A), \mathbb{T}_{Y|A^\ell}(Y^\ell; \theta_Y)) \left| \frac{\partial \mathbb{T}_A(A^\ell; \theta_A)}{\partial A^\ell} \frac{\partial \mathbb{T}_{Y|A^\ell}(Y^\ell; \theta_Y)}{\partial Y^\ell} \right| \quad (14)$$

$$f_{U_A, U_Y}(U_A^\ell, U_Y^\ell) = \frac{\partial^2 \mathbb{F}_{U_A, U_Y}(U_A^\ell, U_Y^\ell)}{\partial U_A \partial U_Y} = \frac{\partial^2 \mathbb{C}(U_A^\ell, U_Y^\ell)}{\partial U_A \partial U_Y} = \mathbf{c}(U_A^\ell, U_Y^\ell) \quad (15)$$

where $U_A, U_Y \in \mathbb{I}$ with \mathbb{C} and \mathbf{c} denoting the copula and its corresponding copula density function.

Hence, we may use any desired copula from the wide range of families of copulas as discussed in detail in [16, 48, 70]. Recently, there has been interesting works that are identifying the similarities between normalising flows [25, 38, 50, 62, 83] and copula flows such as [17, 29, 37, 39, 89].

Thus, it follows that the assumption of Gaussian copula in ρ -GNF may in theory be relaxed by using any family of copula in place of normalizing flows such as Archimedean copulas [39] (Clayton, Frank, Gumbel, etc.), elliptical, or empirical copulas [5, 16, 48, 70] etc. as recent works in normalizing flows such as [4, 17, 29, 37–39, 46, 89, 93] demonstrate the similarities to copulas. However, if one still opines that the selection of an appropriate copula to be a strong assumption, from the copula decomposition results of [48, 91, 94], the unknown copula $\mathbb{C}(U_A, U_Y)$ maybe represented as a convex sum of Frèchet bound copulas $W(U_A, U_Y) = \max(U_A + U_Y - 1, 0)$, i.e., countermonotonicity copula and $M(U_A, U_Y) = \min(U_A, U_Y)$, i.e., comonotonicity copula and the independent/product copula $\Pi(U_A, U_Y) = U_A U_Y$ as below,

$$\mathbb{C}(U_A, U_Y) = \lambda_W W(U_A, U_Y) + \lambda_M M(U_A, U_Y) + (1 - \lambda_W - \lambda_M) \Pi(U_A, U_Y) \quad (16)$$

where $0 \leq \lambda_W, \lambda_M \leq 1$ and $\lambda_W + \lambda_M \leq 1$ such that λ_W and λ_M represent the respective composition/proportion of comonotonic and countermonotonic dependence between U_A and U_Y in $\mathbb{C}(U_A, U_Y)$. Instead of ρ as only one tunable sensitivity parameter with the Gaussian copula, we have two sensitivity parameters λ_W and λ_M to approximate the unknown copula \mathbb{C} . Observe that for Gaussian copula $\mathbb{C}(U_A, U_Y) = \Phi_\rho(\Phi^{-1}(U_A), \Phi^{-1}(U_Y))$ with $\rho = -1$ and $\rho = +1$ respectively correspond to copulas W and M [44]. Thus, the decomposition of the copula \mathbb{C} into W , M and Π copulas may be attributed as

- $W(U_A, U_Y) : \rho = -1$ or $\{\lambda_W = 1, \lambda_M = 0\}$ in Eq. (16).
- $M(U_A, U_Y) : \rho = +1$ or $\{\lambda_W = 0, \lambda_M = 1\}$ in Eq. (16).
- $\Pi(U_A, U_Y) : \rho = 0$ or $\{\lambda_W = 0, \lambda_M = 0\}$ in Eq. (16).

Hence, we see that the assumption of Gaussian copula is not a limitation and can be replaced with any desired copula \mathbb{C} or its decomposition from Eq. (16). Deep Archimedean Copulas [39] are also recently proposed for deep-learning inspired Archimedean copula modeling from observational dataset. We leave the exploration of these alternate techniques of choosing and assuming copulas as motivated above to future work.

7 Implementation level details of our sensitivity analysis experiments

As mentioned in Section 3, we perform experiments in three different settings. In our simulated setting, we consider both continuous and binary outcome variables. In our first simulated setting, we

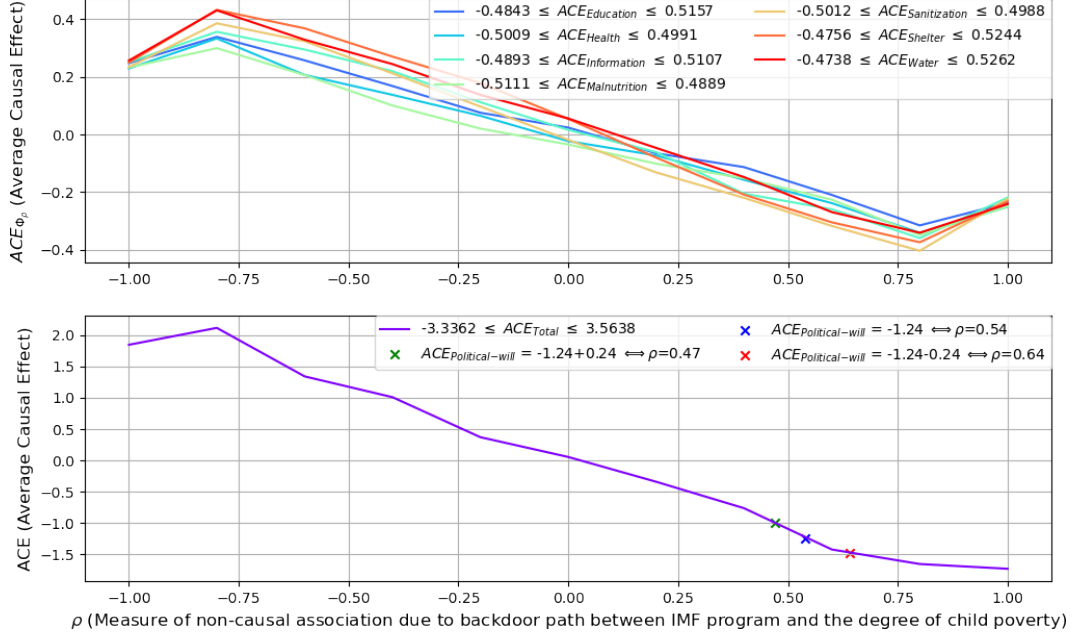


Figure 5: ρ_{curve} generated for each of the individual dimensions of the child poverty as well as the categorical outcome, i.e., total degree of the child poverty with their respective AF bounds obtained on in the IMF child poverty dataset. The point $(\rho, ACE_{\rho}) = (0.54, -1.2)$ corresponds to the ACE estimate from [2] obtained under observed confounding due to political-will of a country.

consider the SCM in Eq. (8) with continuous outcome variable and in our second simulated setting, we consider the data generating processes from [58, 73, 75] with binary outcome variable. In our simulated experiments, we generate 50000 samples from the respective DGPs and randomly split the dataset into train, validation and test sets in the ratio 8:1:1. In our real-world experiments, we consider the IMF dataset from [3, 11, 12, 23] with 1,941,734 children under the age of 18, cared for by 567,344 families residing in 67 countries from the Global-South. The original DAG consists of 32 observed variables such as economy, polity, public spending, living condition, etc. along with the observed IMF program treatment at a country level and the degree of the child poverty under the observed treatment to adjust for the confounders for the ACE estimation. The degree of the child poverty in the dataset is calculated based on the simple sum of 7 individual dimensions of poverty for each of the child, i.e., (i) education, (ii) health, (iii) information, (iv) malnutrition, (v) sanitization, (vi) shelter, (vii) water, resulting in an aggregate degree of child poverty between 0 and 7 with 0 indicating no poverty and 7 indicating severe poverty. Due to the sensitive nature and the accompanying ethical considerations, the complete IMF dataset is not made publicly available and can be requested upon from the authors of [3, 11–14, 23]. Since, our sensitivity analysis does not require any confounding to be observed, we do not access any of the macro- and micro- socio-economic factors. We only consider the observed IMF program as the treatment A and the observed total degree of child poverty as the outcome of interest Y . Since deep neural networks are prone to overfit, we split the data into 1,922,316 training, 9,709 validation and 9,709 test samples.

For all the three experimental settings, we strictly use only the training set samples for training and use the held-out validation set for early stopping to get the model with best validation loss. We further validate the generalization of the best validation loss model on the held-out test set. We use fully-connected layers with [20, 15, 10] hidden units for the graphical conditioner and fully-connected layers with [15, 10, 5] hidden units for the monotonic UMNN transformer. We implement c-GNFs in PyTorch [51] using GNF [88] baseline code and AdamW [40] optimizer with learning-rate= $3e-4$ and a batch-size of 128 (2GB of GPU memory) per simulation in all our experiments. Our supplemental material consists of the codes to run all the three experimental settings.

7.1 Assumption-Free Bounds for the Degree of Child Poverty categorical outcome

Observe that unlike the binary outcomes, AF bounds are not available for the non-binary outcomes such as the IMF child poverty dataset. However, as mentioned earlier the total degree of child poverty is formulated as the sum of the seven binary variables that represent the individual dimensions of the child poverty, i.e., (i) education, (ii) health, (iii) information, (iv) malnutrition, (v) sanitization, (vi) shelter, (vii) water. Fortunately, since these binary outcomes are observed and the actual categorical outcome, i.e., the total degree of the child poverty is a simple sum of these seven binary variables, we may identify the lower and upper bounds of the total degree of child poverty as a results of lower and upper bounds of the summations of the individual dimensions of child poverty.

From the Fig. 5, we see that the lower and upper bounds of the total degree of child poverty is identified as $[-3.3362, +3.5638]$ from the AF bounds of the seven individual dimensions of child poverty, (i) education: $[-0.4843, 0.5157]$, (ii) health: $[-0.5009, 0.4991]$, (iii) information: $[-0.4893, 0.5107]$, (iv) malnutrition: $[-0.5111, 0.4889]$, (v) sanitization: $[-0.5012, 0.4988]$, (vi) shelter: $[-0.4756, 0.5244]$, (vii) water: $[-0.4738, 0.5262]$. We see that our narrower empirical bounds of $[-1.7, 2.1]$ is indeed within the AF bounds of $[-3.3362, +3.5638]$. Observe that the ρ_{curve} and the $\rho_{value} \cong 0$ helps us further narrow the bounds to $[-1.7, 0]$, i.e., $ACE_{\rho} < 0$ under the reasoning that the confounding between the IMF program and the degree of child poverty is positively correlated as presented in Section 3.3. Effectively, instead of the uninformative widest AF bounds width of 7, we obtain a narrower width of 1.7, i.e., a reduction of the bounds by 75.7% which is really informative to the analyst/domain-expert. This narrower bound is obtained at the expense of the injection of the domain knowledge in the form of Gaussian copula assumption and the positively correlated confounding assumption. If, we assume only the Gaussian copula assumption by excluding the positively correlated confounding assumption, we obtain a narrower width of 3.8, i.e., a reduction of the bounds by 45.7% which is also informative to the analyst/domain-expert in comparison to the uninformative widest AF bounds width of 7.

8 Validation of Gaussian dequantization trick implementation in PyTorch

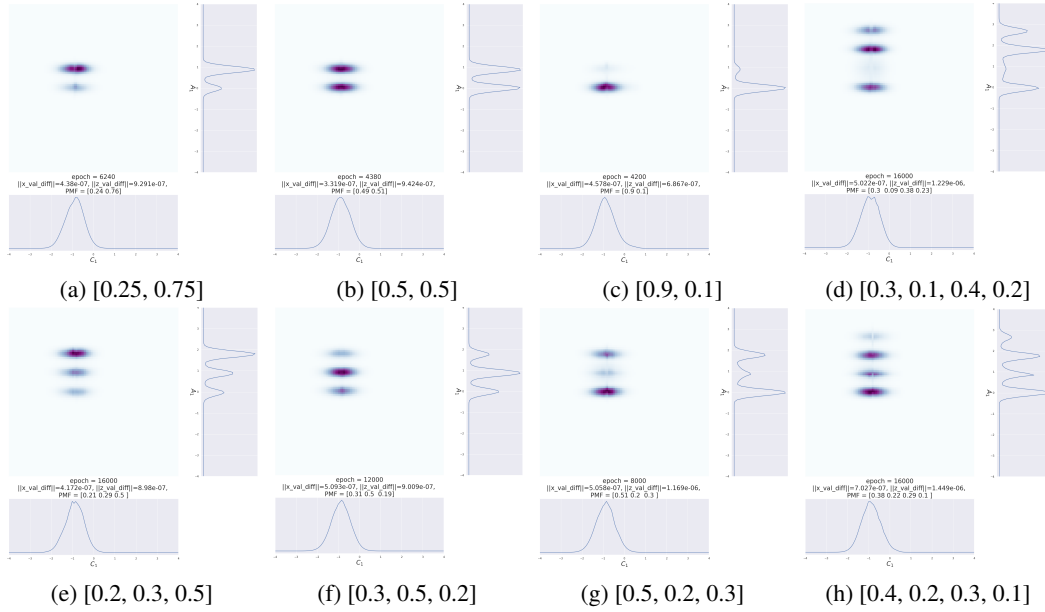


Figure 6: (a, b, c) present categorical variable A_1 with 2 categories/classes represented by different class probabilities. Similarly, (e, f, g) present categorical variable A_1 with 3 categories/classes represented by different class probabilities. (d, h) indicates A_1 with 4 categories/classes represented by different class probabilities. We observe our implementation to be correct and thus validate the Gaussian dequantization trick irrespective of the number of categories or the ordering of the categories.

In Fig. 6, we observe the simultaneous implementation of the continuous variable ($C_1 \sim N(-1, 0.5)$) and discrete variable (A_1 with respective probability mass functions) in the same ρ -GNF using our PyTorch implementation of the Gaussian dequantization trick from c-GNF [3]. The verification is done by observing the area under each of the individual modes as the probability mass corresponding to the discrete variable. We see visually present the verification of our implementation of Gaussian dequantization to be able to satisfactorily model both continuous and discrete simultaneously.

9 Additional plots of ACE along with the expected potential outcomes as a function of different ρ -GNF

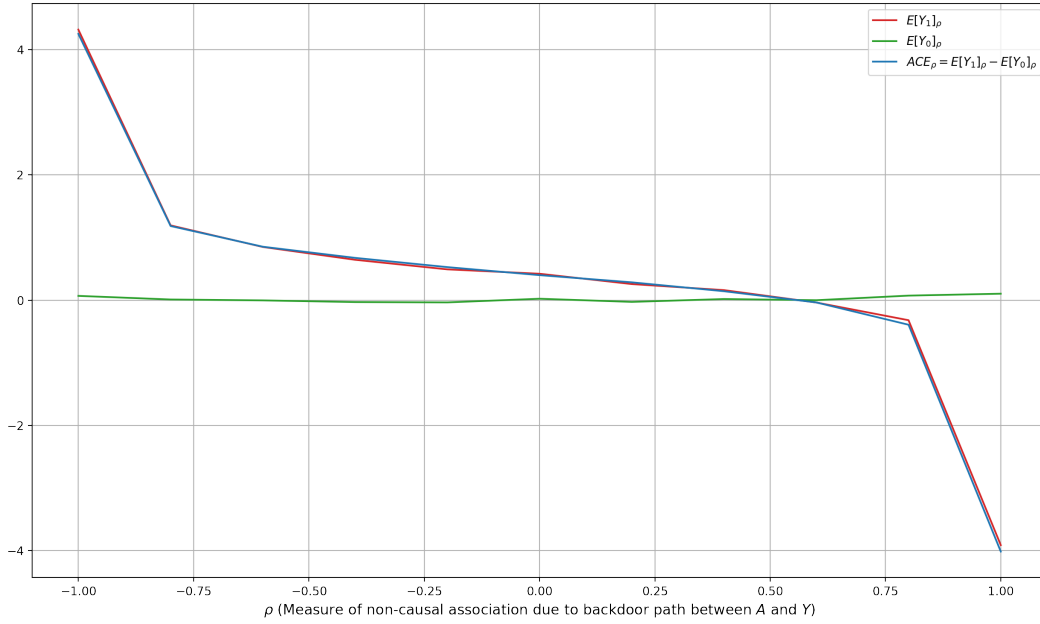


Figure 7: ρ_{curve} generated for observational data from $SCM_{0.0,0.55,0.55}$ with the continuous outcome Y presented in Fig. 2b. As expected, $\mathbb{E}[Y_0]_\rho$ is zero, which makes $ACE_\rho = \mathbb{E}[Y_1]_\rho$, where $\mathbb{E}[Y_1]_\rho$ may follow arbitrary function determined by the observational dataset and the value of ρ .

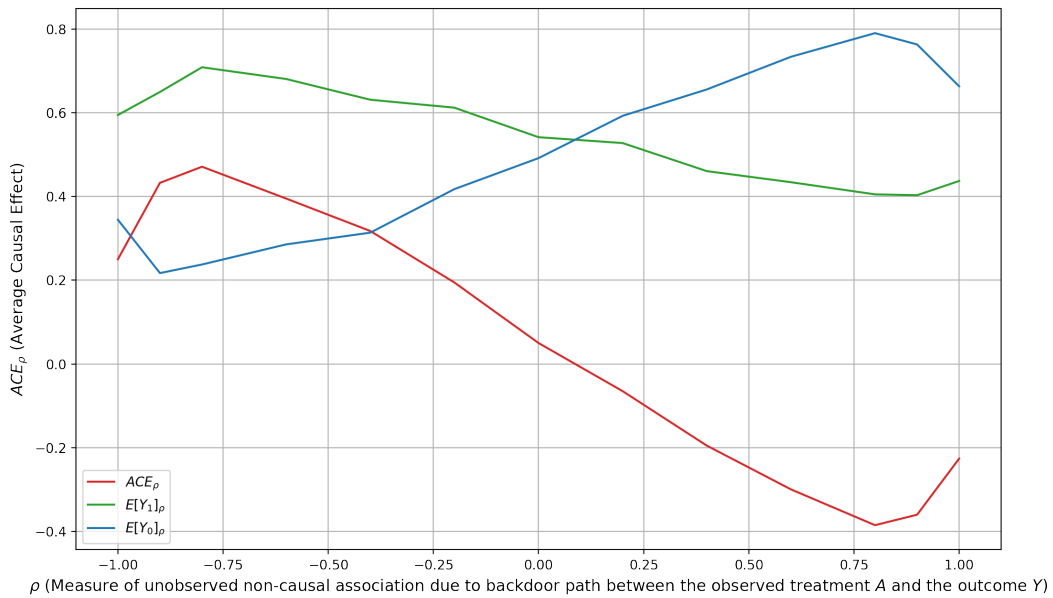


Figure 8: ρ_{curve} generated for observational data presented in Fig. 3 from the DGP (row 2, column 3) with the binary outcome Y . Unlike the case of continuous outcome in Fig. 2b and 7, both $\mathbb{E}[Y_0]_\rho$ and $\mathbb{E}[Y_1]_\rho$ determining ACE_ρ may follow two arbitrary function determined by the observational dataset and the value of ρ . Especially, the observed decrease/increase in ACE_ρ corresponds to the respective decrease/increase in $\mathbb{E}[Y_1]_\rho$ and increase/decrease in $\mathbb{E}[Y_0]_\rho$ at the left/right extremes.